Soft Computing (2023) 27:7401–7418
https://doi.org/10.1007/s00500-023-07977-5

OPTIMIZATION

A novel intelligent method to increase accuracy of hybrid photovoltaic-wind system-based MPPT and pitch angle controller

Tao Hai[1,2,3] · Jincheng Zhou[1,4,5] · Sajjad Dadfar[6]

Accepted: 25 February 2023 / Published online: 12 April 2023

Abstract

The main aim of this paper is the optimal power extraction based on an intelligent structure. It is implemented through fuzzy gain scheduling of PID (FGS-PID) controller in combination with the radial basis function network sliding mode (RBFNSM) for controlling a grid-connected hybrid generating system. A wind turbine (WT) based on the permanent magnet synchronous generator (PMSG) and a photovoltaic (PV) is considered for this study. FGS-PID controller equipped with scaling factors (SF) for the input signals of FGS are used to reach MPPT for the PV system. In order to regulate the member functions (MFs) of FGS, the fuzzy logic controller (FLC) and developed farmland fertility optimization (IFFO) algorithm are used. Moreover, the pitch angle control is applied for the WT. The pitch angle control of the WT is implemented by the RBFNSM to control the generated power and the speed at the nominal value. For protecting the wind turbine architecturally and escape catastrophic operation, this idea is implemented. MATLAB software is used to show the effectiveness of the proposed controller. The main advantages of the proposed method over other approaches are efficiency, fast and accurately tracking the highest generated power of the PV system.

Keywords Wind turbine · IFFO algorithm · Hybrid power system · MPPT · Photovoltaic · Fuzzy methods

1 Introduction

Nowadays, energy, in particular electricity, surely constitutes one of the major necessities of daily human life. As the energy demand grows, electricity prices are directly affected by the higher prices of the fossil fuels, such as coal and oil (Veeramanikandan and Selvaperumal 2021). From another perspective, the higher levels of contaminants resulting from fossil fuels have led environmentalists to seek a better alternative and decrease the amount of fossil fuels consumed. A variety of alternatives is available for fossil fuels, such as hydro-power, solar, and wind energies. Each of these energy sources has its own limitations and advantages. Of the whole sources of energy, the electrical power produced by means of solar sources is among the propitious sources of energy, which is easily and widely accessible (Radhika et al. 2020). Soon, solar power will have a major role as a renewable source of energy, which is attributable to its advantages, such as low pollution, low maintenance costs, and easy accessibility (Shengqing et al. 2020).

✉ Jincheng Zhou
guideaaa@126.com

✉ Sajjad Dadfar
sajjad.dadfa.usa@gmail.com

[1] School of Computer and Information, Qiannan Normal University for Nationalities, Duyun 558000, Guizhou, China

[2] State Key Laboratory of Public Big Data, Guizhou University, Guiyang 550025, Guizhou, China

[3] Institute for Big Data Analytics and Artificial Intelligence (IBDAAI), Universiti Teknologi MARA, 40450 Shah Alam, Selangor, Malaysia

[4] Key Laboratory of Complex Systems and Intelligent Optimization of Guizhou Province, Duyun 558000, China

[5] Key Laboratory of Complex Systems and Intelligent Optimization of Qiannan, Duyun 558000, China

[6] Department of Electrical Engineering, Saveh Branch, Islamic Azad University, Saveh, Iran

The major dilemmas encountered in the field of applying photovoltaic systems include their low efficiency and high manufacturing costs due to the nonlinear specifications of the I–V curves (Khan and Mathew 2021). The output power obtained from each solar cell is directly affected by the intensity of the solar radiation, while it is conversely related to the temperature, and both of these parameters are subjected to changes over time. As a result, MPP tracking techniques must be used to overcome such changes (Khan and Mathew 2021). During the last decade, a great number of techniques have been suggested for the purpose of MPPT applications. A number of them include incremental conductance (Luo et al. 2020), perturbation and observation, fuzzy logic control, ripple correlation control, and short-circuit current extremum-seeking control techniques (Dadfar et al. 2019).

Among the aforementioned methods, the perturbation and observation technique is regarded as a commonly used method, which functions on the basis of voltage perturbation by applying the previous operating power P_{old} and the present P. In the case that the power generated by the photovoltaic system is increased, i.e., the operational point moves toward the maximum power point, in the next exploitation voltage, a perturbation will be generated in alignment with the preceding exploitation voltage. The same operation is continued until reaching MPP; however, the decreased power received from the photovoltaic system means that it is far from MPP, and as a result, one should change the perturbation direction (Hosseini and Rezvani 2020). Even though this technique is very simple, its efficiency is highly dependent on the fluctuations around MPP and convergence speed due to the fact that if the speed of convergence is increased, the accuracy of the convergence declines, while fluctuations around MPP are increased. As a result, the parameters are required to be modified in such a way that neither fluctuation is high around MPP nor convergence speed is low (Hai et al. 2022). Another big challenge is the rapid changes in irradiance for the P&O technique, which may potentially lose its direction in spite of tracking the true MPP. The incremental conductance (INC) method outperforms the P&O for variable step increments. Nonetheless, its drawback is exhibiting power oscillations near the optimal power point (Izadbakhsh et al. 2015).

One of the most robust intelligent controllers for photovoltaic systems is the FLC MPPT. This is attributable to its lesser oscillations and high response in comparison with the conventional MPPT technique. Also, it has been regarded as efficient and effective equipment used to manage systems' nonlinearities and uncertainties (Li et al. 2019; Salameh et al. 1991). However, its major limitation is the drift problem related to the changes observed in the irradiation levels and temperature operation. This is due to the fact that it is heavily dependent on a good knowledge of photovoltaic systems, leading to imprecise membership functions (Mahmoud and Oyedeji 2018).

The rated power generation of large wind turbines would be controlled through controlling the pitch angle at the root of the blade. Any actuation of the pitch angle would result in considerable oscillations in the blade load of the turbine inversely impacting the power generation, stability and also life time of the turbine. Pitch-adjusting variable-speed WTs have already turned into the most interesting option for the wind energy systems during these years. In this regard, two controllers are available for such systems cross-coupled each other. For the speeds lower than the cut-in speed, the rotor speed can be uninterruptedly tuned to keep the TSR unchanged at a point resulting in the highest power coefficient. Consequently, the system efficiency would also go up. It is worth noting that even a little pitch angle variation leads to considerable change in the output. According to Hai et al. (2023), the pitch angle control is performed to meet the following goals: (i) Achieving the optimal WT's output. (ii) Avoiding the mechanical power at the input to surpass the system limits. (iii) Lowering the WT mechanical element fatigue where the control system can influence the load, and the effect on the load should also be considered when designing the system. It is worth mentioning that the design of the control system can be in a way to mitigate a certain fatigue load considered as another aim.

There are many research works devoted to controlling the hybrid power systems, including wind and solar PV (Hong and Chen 2014), while ref (Oskouei et al. (2016)) also considered the battery system to this end. Reference (Benadli and Sellami 2014) investigated the problem of optimal control of a hybrid generating system with a WT and a PV operating in the islanded mode using a sliding mode control. A large number of publications tried to utilize wind farms comprising doubly fed induction generator-based WTs together with a PV in the form of a hybrid system (Parida and Chatterjee 2016). The use of DFIG-based WTs in a hybrid PV-wind unit brings numerous merits among which simplicity, separated active and reactive power control, partially rated converters and the capability of extracting the highest output are the most significant ones (Kumar et al. 2014). To supply distant regions, a PV-DFIG hybrid power system has been suggested in Rajesh et al. (2015). In Rajesh et al. (2015), a tool has been developed to analyze a hybrid PV-wind generating. To improve the power quality and extract the highest output from the hybrid generating system, several control schemes are also proposed in the literature. An improved P&O MPPT method to obtain the highest power using a grid-connected hybrid generating unit has been developed in Sera et al. (2013).

It is noteworthy that since no solar irradiance is available at night and the output of the solar PV panels changes as a result of the varying solar irradiance during the day, it cannot satisfy the required power generation demand all over the day. Consequently, it would not be possible to generate power continuously unless such an operation is conducted jointly with storage systems, such as commonly used wind turbine (WT) systems. While the use of this system as a hybrid energy system can be of great help in stabilizing power and overcoming the power output volatility associated with solar photovoltaic systems, it is cost-effective. Nonetheless, in spite of the declining cost of manufacturing hybrid PV-WT systems, a remaining controversial issue is the payback period of these systems (Mahmoud and Oyedeji 2018).

- The recommended system is capable of effective tracking of the MPP and, thus, extraction of the maximum power.
- The combination of the algorithm of improved farmland fertility optimization (IFFO) and the fuzzy logic controller (FLC) is used in order to fine-tune the member functions (MFs) of FGS.
- The RBFNSM is used for the pitch angle control of the WT to restrict the generated power and the speed at the nominal value to protect the wind turbine structurally and avoid catastrophic operation.
- The main advantages of the presented FGS-PID-IFFO MPPT technique include high accuracy, rejection of reference voltage oscillations, and shorter tracking time.

The remaining of the study is as follows: Section 2 represents PV cell. Section 3 shows MPPT method. IFFO algorithm and WT method are given in Sect. 4 and Sect. 5, respectively. The P-Q controller and simulation results are given in 6. Lastly, conclusions are provided.

2 Presented model

2.1 Photovoltaic system

Solar power plants around the world are made up of basic components called solar cells. Solar cells can be combined in different forms in series or in parallel to form solar arrays at the desired power and voltage rating (Izadbakhsh et al. 2015). There are several methods for modeling a solar cell. Here, to simplify, the single-diode model is used according to Fig. 1 (Li et al. 2019). The voltage and current relationships of this modeling are described below:

$$I_{\mathrm{PV}} = I_{\mathrm{ph}} - I_{\mathrm{PV0}}\left[\exp\left(\frac{q(V_{\mathrm{PV}} + I_{\mathrm{PV}}R_{\mathrm{s}})}{n\mathrm{KT}} - 1\right)\right] - \frac{V_{\mathrm{PV}} + R_{\mathrm{S}}I_{\mathrm{PV}}}{R_{\mathrm{sh}}} \quad (1)$$

where V_{PV} is the output voltage. Table 1 represents PV characteristic.

3 MPPT schemes

The present research work uses different items from the prevalent controller as well as adaptive ones as the main components of the MPPT algorithm. The developed MPPT technique performs on the basis of the bi-level fuzzy control, which is capable of being used in every control scheme using the error (Chopra et al. 2005). It is worth mentioning that a prevalent PID controller can be supervised using the flexible FGS. In this respect, fuzzy-based PID controllers are clustered in three main groups as FGS, hybrid fuzzy PID controller, and also the direct action ones (Ogata 2022). The proposed FGS-PID scheme is categorized into the first groups. Moreover, as Fig. 2 depicts, this controller may be employed with adaptive scaling factors.

3.1 The Z-N method

The gain of PID controllers can be tuned using intelligent optimization algorithms or conventional methods (Harrag and Messalti 2015; Ahmadi et al. 2017). The GA, ant colony algorithm (ACA), bacterial foraging algorithm (BFA), BAT search method, and artificial bee colony algorithm (ABCA) are some examples of optimization algorithms. However, low convergence rate, as well as being trapped into local optima, is the main disadvantage of these methods. The empirical scheme, upward curve technique, critical ratio method, and relay feedback method are also some of the popular conventional methods. Among different conventional methods, the Z-N approach is a mature and strong technique, which is presented by Ziegler and Nichols in a seminal paper. The Z-N approach is implemented on the basis of two philosophies, including characterizing process dynamics using two parameters.

3.2 Conventional regulator

The continuous-time relation of the PID controller in this research work can be stated as follows:

$$G(s) = K_{\mathrm{p}}\left(1 + \frac{1}{T_i s} + T_{\mathrm{d}} s\right) \quad (2)$$

The gain relating to the proportional controller of the PID is indicated by K_{P}, while the time constants of the

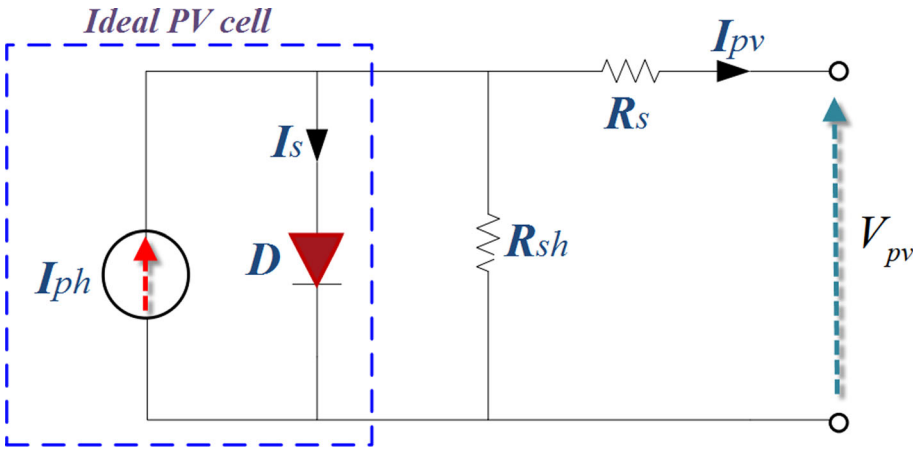

Fig. 1 Solar cell modeling

Table 1 PV characteristic

Maximum current	Maximum voltage	Maximum power	Open circuit voltage	Short circuit current
4.94 A	18.65 V	90 W	22.32 V	5.24 A

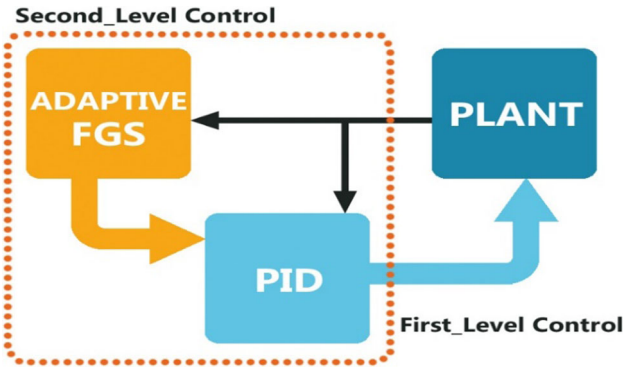

Fig. 2 Configuration of bi-level control system

integral and derivative parts are indicated by T_i and T_d, respectively. In addition, the gains of the integral and derivative parts are determined as $K_i = K_P / T_i$ and $K_d = K_P T_d$, respectively. In order to optimally tune the PID gains, the Ziegler-Nichols reaction curve approach is used (Chopra et al. 2005). Hence, the PID can be optimally tuned using the optimal values of the gains. Moreover, the optimal values of the operating parameters, including the rise time, the settling time, and the percentage overshoot, respectively, shown by t_r, t_s, and M_p in addition to the steady-state offset, etc., can be attained.

3.3 FGS-PID MPPT

The dynamic performance of the solar PV in various conditions highlights the need for enhanced control methods. The above-cited PID-based MPPT approach does not have the capability to appropriately deal with various operating conditions. Thus, this paper presents an online tuning of the PID controller for the real-time MPPT scheme.

3.4 FGS-PID control scheme

FLC is a tool capable of handling either linear or nonlinear systems, and it has a simple configuration with high efficiency. The FLC has a considerably better performance compared to prevalent controllers for nonlinear systems, while it has the capability of operating properly even with the imprecise inputs. In this respect, fuzzy logic is taken into account a supervised learning approach that has the relatively same procedure as the way a human thinks and the language used by the human. This technique is capable of dealing with the uncertainty and also uncharacterized systems. Furthermore, inaccurate parameter values can be effectively handled, and it provides even transitions between the systems. This technique has been thus far extensively used to tune the gain of the controllers. In this respect, once the system conditions vary, the gains of the controller can be efficiently readjusted by the controller according to the rules known as "IF–THEN" rules. Accordingly, this research work employs the fuzzy logic using the Mamdani's approach due to its numerous merits to tune the PID controller gains in a framework known as the FGS-PID control framework. The above-mentioned system is presented in the following where it should be noted that the derivative time constant changes the integral time constant.

$$T_i = aT_d \tag{3}$$

$$K_i = \frac{K_p}{aT_d} = \frac{K_p^2}{aK_d} \quad (4)$$

$$K_p = K_p^{'}(K_{p,max} - K_{p,min}) + K_{p,min} \quad (5)$$

$$K_d = K_d^{'}(K_{d,max} - K_{d,min}) + K_{d,min} \quad (6)$$

The conceptual procedure of the proposed FGS-PID is illustrated in Fig. 3.

It is noteworthy that the variations range of the error and also the change of error should be in the interval [–1 1]. Using the trial and error, it is possible to determine the desired scale factors, as stated in the following.

3.5 Adaptive FGS-PID controller

Figure 4 illustrates the conceptual structure of the proposed FGS-PID system with adaptive scaling factors. In this regard, some fuzzy rules are required, while they are determined using the mentioned trial and error approach prior to getting to the intended operating level. This method may be associated with a considerable computational burden, and it may take longer for an inexperienced designer. This problem mainly relates to the varying conditions of the system, which makes it complicated to tune the parameters. It is highly needed to design a framework for online tuning to meet the desired dynamic performance. There are numerous research works thus far devoted to designing autonomous tuning of controllers utilizing the fuzzy logic (Mudi and Pal 1999; Zhao et al. 1993). These research works tuned only the output SF or for prevalent PID controllers. It should be noted that as the input scaling factors in FLCs impact the operation and the controller, they should be optimally tuned (Chopra et al. 2005). Hence, this paper presents an autonomous tuning technique for FLCs. Utilizing some updating factors that their values are specified using rule base with the error and the change of the error as the inputs with respect to the needed controlled performance, the input scale factors can be adjusted online. It is worth mentioning that this technique would not teach the rue base of the FLC, and it supposes a set of rules to adjust the controller to meet an intended performance level. Reference (Leng et al. 2018) is used for the rules as well as the membership functions of α and β with a little change to tune the FLC over the MPPT. Figures 5 illustrate the membership functions taking into account α and β, as well as E(k) and CE(k). The rules used for α and β are represented in Table 2. Besides, novel membership functions are used for the gain of α varying in the interval [-0.5 and 3] aimed at incrementing the sensitivity of α fuzzy rule sets to fast diagnose the remarkable variations of the output influenced by the alteration of the solar irradiance. It is noted that the trial and error approach is used to specify the domain of gain factor α leading to the desired results.

4 Optimization of fuzzy PID

4.1 Adaptive FLC

The conventional fuzzy logic controller technique suffers from serious challenges in selecting member functions. One can use swarm optimization techniques in order to overcome the same challenge. The present paper employs improved farmland fertility optimization in order to regulate the MFs of the fuzzy logic controller. This technique can bring about fast-paced attainment to the MPP. For this reason, the cost function is introduced via the integral time absolute error (ITAE) criteria:

$$\text{ITAE} = \int_0^{\infty} t \times |e(t)| \mathrm{d}t \quad (7)$$

4.2 IFFO algorithm

As a substrate, the soil is regarded as the most critical factor. The soil texture composition is the first thing to

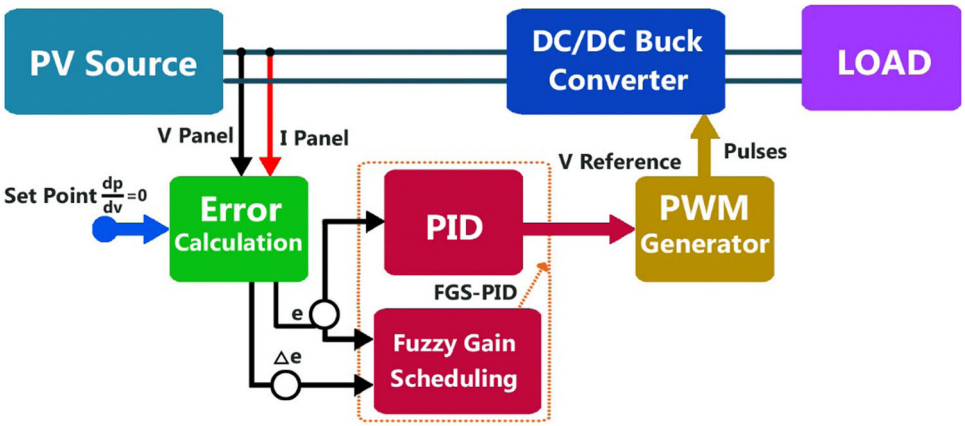

Fig. 3 Conceptual scheme of a PID-based PV system

Fig. 4 FGS-PID scaling factors

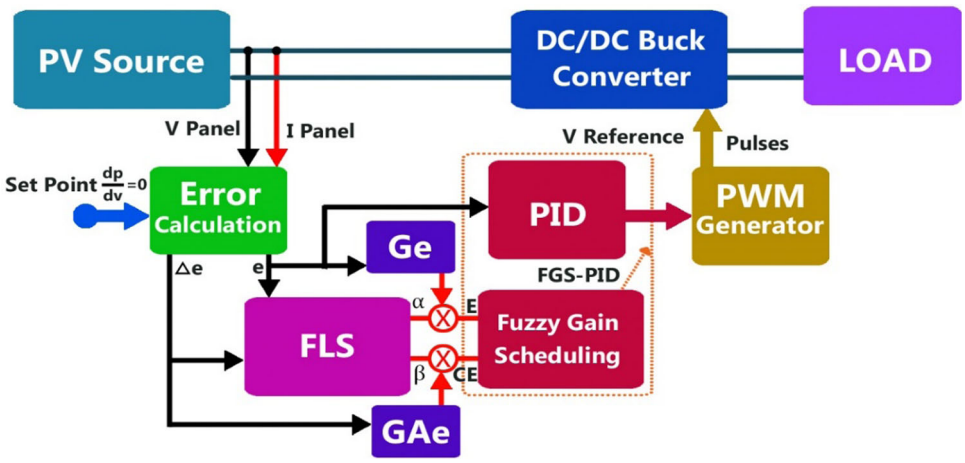

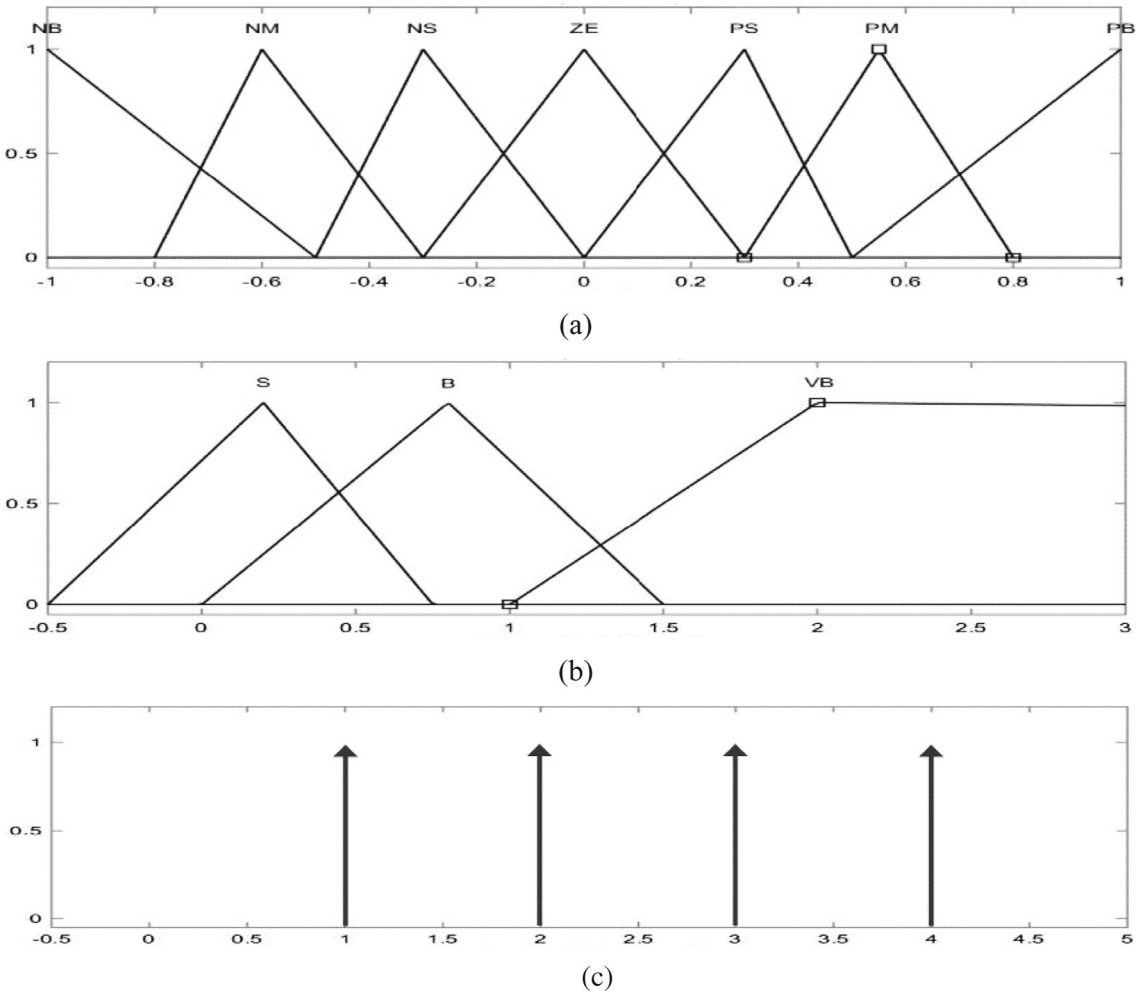

Fig. 5 Membership functions for **a** E and CE **b** α **c** β

consider in order to have an ideal farm. The best type of soil is characterized by the right composition of sand, clay, fertilizer, and silica. The retention of water is difficult in light or sandy soils. From another perspective, extraction/drainage of excess water becomes difficult in clay soils characterized by a high water retention capacity. An ideal combination that creates fertile soils is the use of the right mixture of soil compost or animal manure and these two types of soil (i.e., loamy and sandy). Simply put, the soil is considered fertile from an agricultural viewpoint when it is

Table 2 Rules base for α, β

E(k)								
		NB	NM	NSS	ZE	PS	PM	PB
CE(k)	NB	B,S	VB,S	B,S	B,S	B,S	B,S	B,S
	NM	B,M	VB,M	B,S	B,S	B,S	B,M	B,M
	NS	B,B	VB,M	B,M	S,S	B,M	B,M	B,B
	ZE	B,VB	VB,VB	S,B	S,S	S,B	VB,VB	B,VB
	PS	B,B	VB,M	B,M	S,S	B,M	VB,M	B,B
	PM	B,M	B,M	B,S	B,S	B,S	VB,M	B,M
	PB	B,S	B,S	B,S	B,S	B,S	VB,S	B,S

capable of providing sufficient nutrients for the purpose of plant growth, the results of which are quality products and a higher yield. For the same purpose, through a lot of trials and errors, farmers are seeking an optimized soil composition by combining a variety of ingredients in order to enhance the quality of farmland soils (Shayanfar and Gharehchopogh 2018). For the same purpose, a novel metaheuristic approach has been proposed to overcome optimization dilemmas (Sabo et al. 2020). This newly developed technique is known as the algorithm of farmland fertility optimization (FFO). As a matter of fact, metaheuristics are regarded as some types of model-free techniques used to solve a variety of optimization problems and

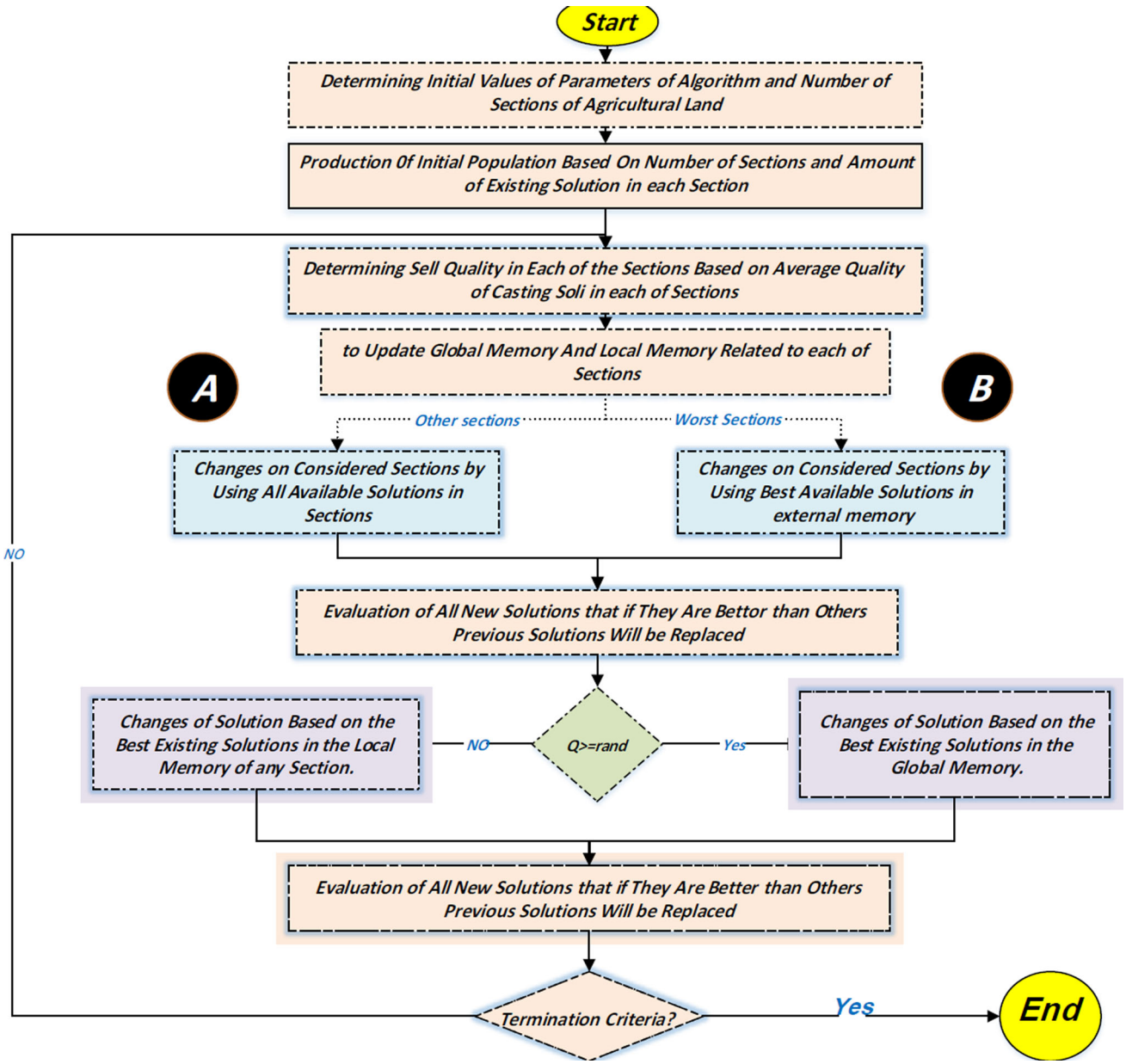

Fig. 6 Flowchart of farmland fertility

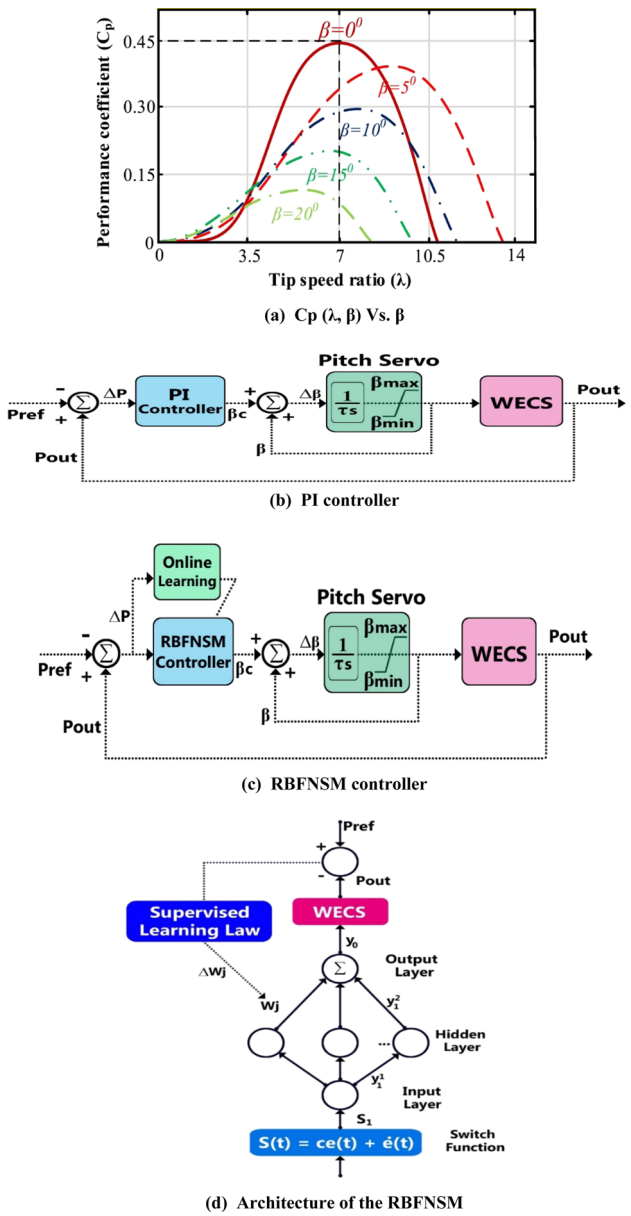

Fig. 7 **a** Cp (λ, β) Vs. β **b**. PI controller **c**. RBFNSM controller **d**. Architecture of the RBFNSM

employed for many applications recently. The farmland fertility optimization algorithm is composed of six major phases, which are briefly described below.

Step 1) Initialization: In the course of the same phase, the number of sections (k) and the applicable solutions for those sections (n) in the farmland are determined. In this respect, one can model the population (N) of the algorithm as below:

$$N = k \times n \tag{8}$$

in which k stands for a positive digit within the [1, N] range that define an integer number. Its selected value in the present investigation is 2, which is determined through trials and errors. The equation below is chosen so as to create the initial individuals within the applicable range.

$$X_{ij} = L_j + (U_j - L_j) \times \delta \tag{9}$$

in which δ symbolizes a random value within the [0, 1] range, and U_j and L_j stand for the upper and the lower limits in the dimension j.

Step 2) Evaluation of the soil quality in all farmland sections: In the same phase, the farmland decision variables are directed in the sections. Then, the value of the cost function is calculated for these decision variables. In much the same way, the quality of soil is determined using the equation below:

$$S_s = X(aj), a = n * (s-1) : n \times ss = [1, \ldots, k], j = 1, 2, 3, 4. \tag{10}$$

Step 3) Updating memory: In this phase, the local and global memories are updated.

$$M_{\text{local}} = \text{round}(t \times n) \tag{11}$$

$$M_{\text{Global}} = \text{round}(t \times N) \tag{12}$$

in which t ∈ [0.1,1], and M_{Global} and M_{local} stand for the number of solutions stored within global and local memories, respectively.

Step 4) Variation of soil quality for every single section: The quality pertaining to each section is determined, and the best quality will be stored within the local memory. In addition, the optimum solution will be stored within the global memory.

$$X_{\text{new}} = h \times (X_{ij} - X_{\text{MGlobal}}) + X_{ij} \tag{13}$$

in which X_{ij} stands for a worst-case, which is adopted for the updating process, X_{MGlobal} stands for a random value through global solutions, and h expresses a decimal number as below:

$$h = \alpha \times r_1 \tag{14}$$

in which a symbolizes a constant value within the [0, 1] range, and r_1 symbolizes a random value within the [–1, 1] range. In order to update other solutions,

$$X_{\text{new}} = h \times (X_{ij} - X_{\text{MGlobal}}) + X_{ij} \tag{15}$$

$$h = \beta \times r_2 \tag{16}$$

in which r_2 symbolizes a random value within the [0, 1] range, and β symbolizes a constant value within the [0, 1] range assumed at the start of the farmland fertility.

Step 5) The composition of soil: Upon determining the best local solutions (L_{best}), farmers select the best soil combination for the farmland. The present phase is modeled mathematically by means of the following equation:

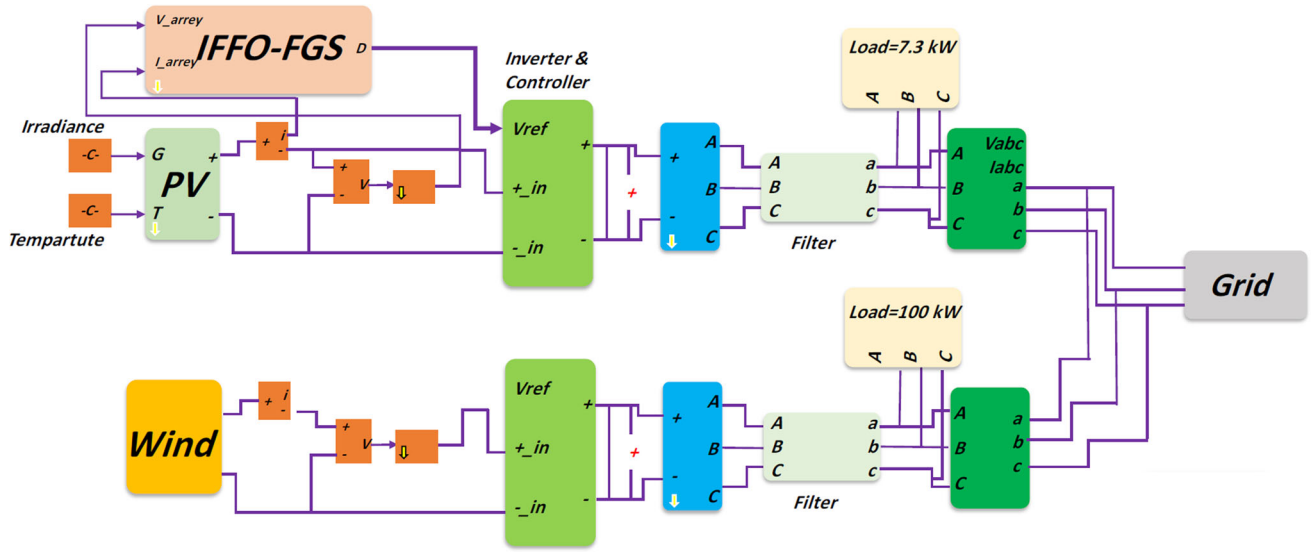

Fig. 8 Proposed system

Fig. 9 **a** Irradiance **b** Temperature

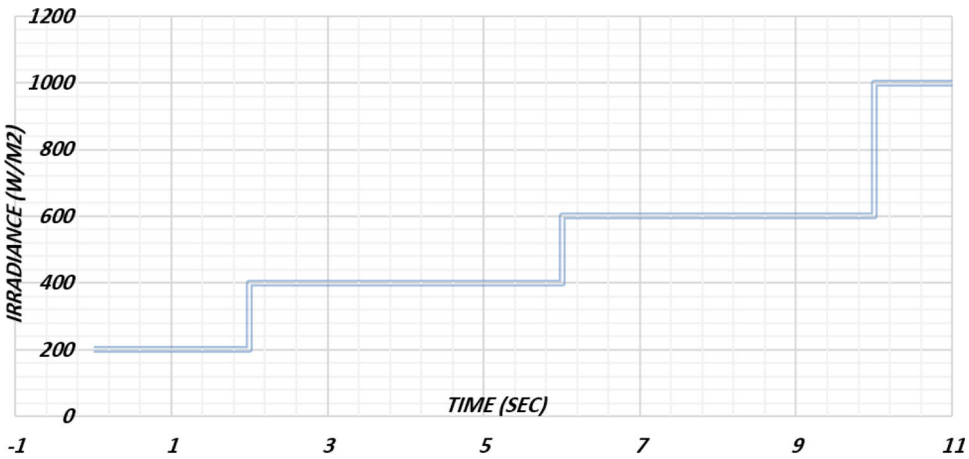

(a) Irradiance

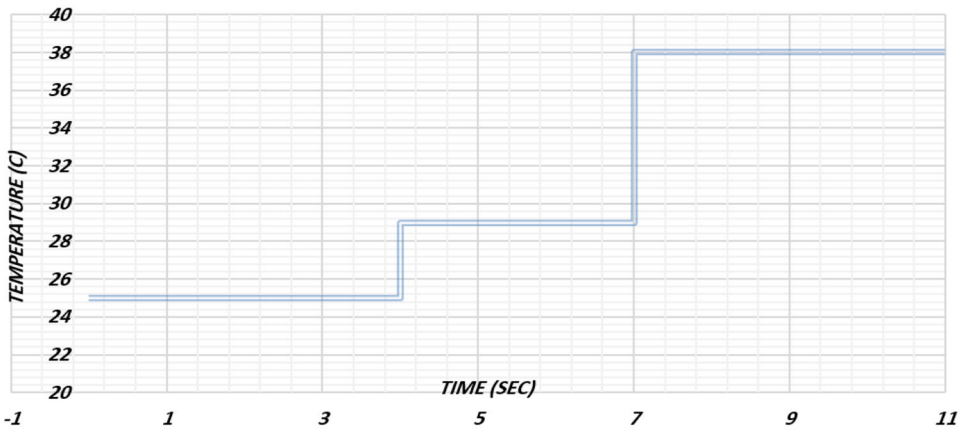

(b) Temperature

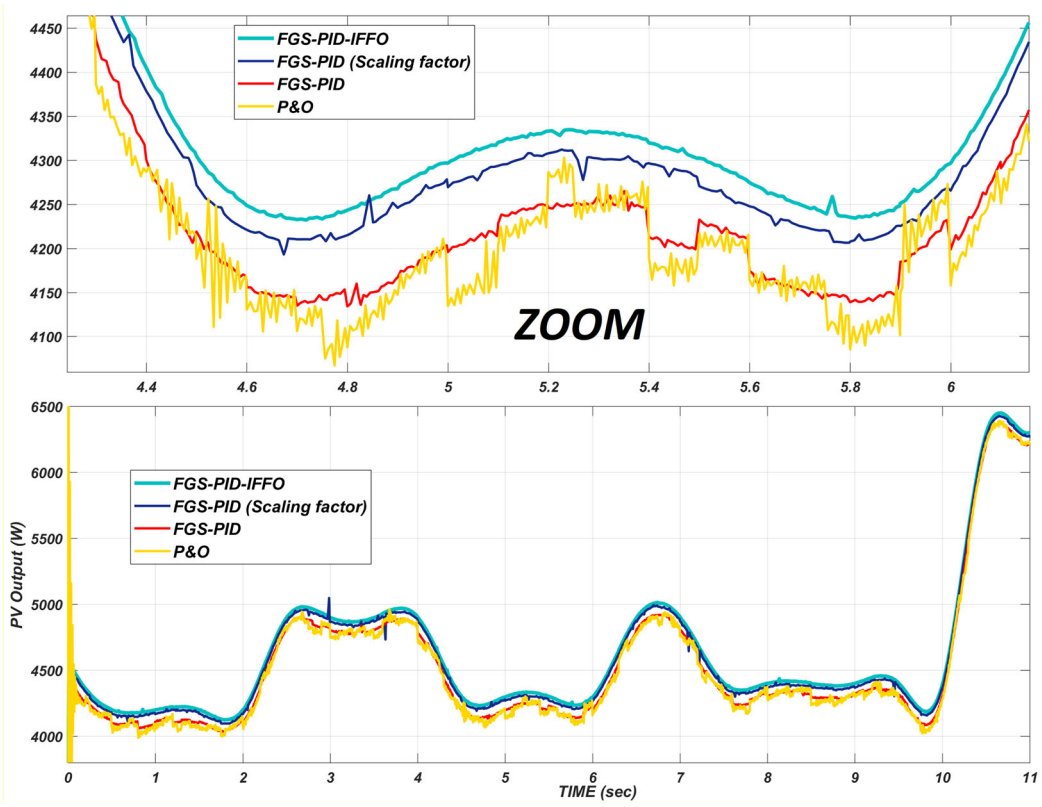

(a)

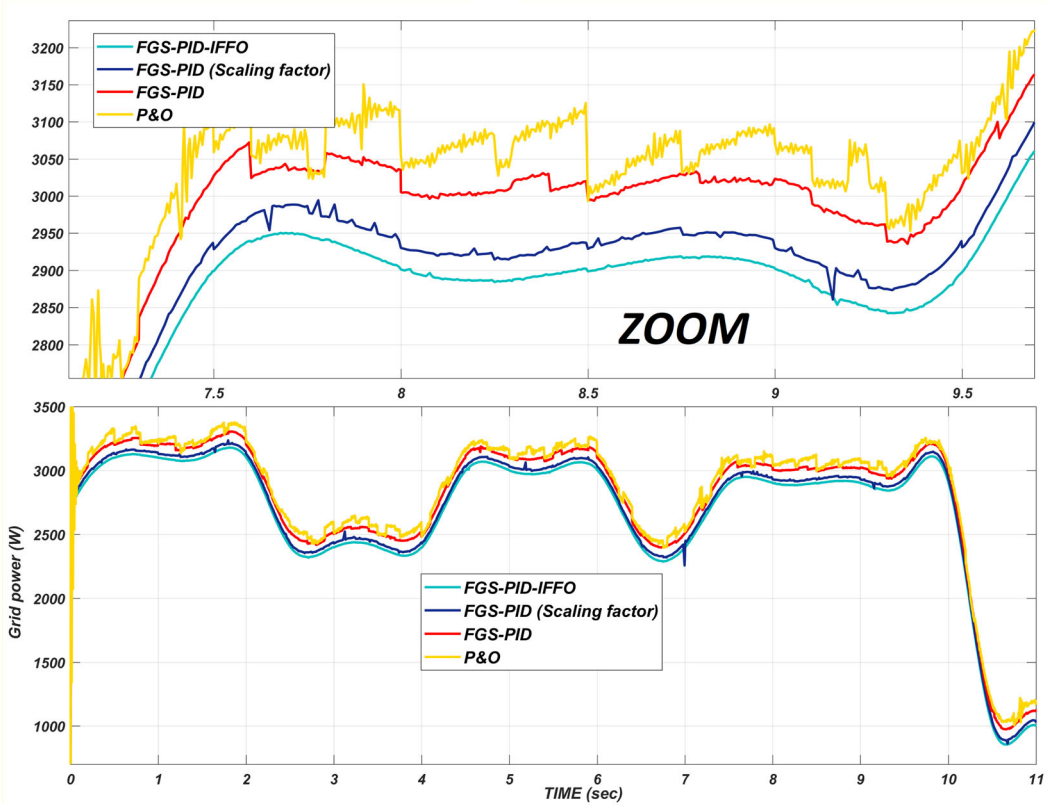

(b)

Fig. 10 **a** PV power; **b** Grid

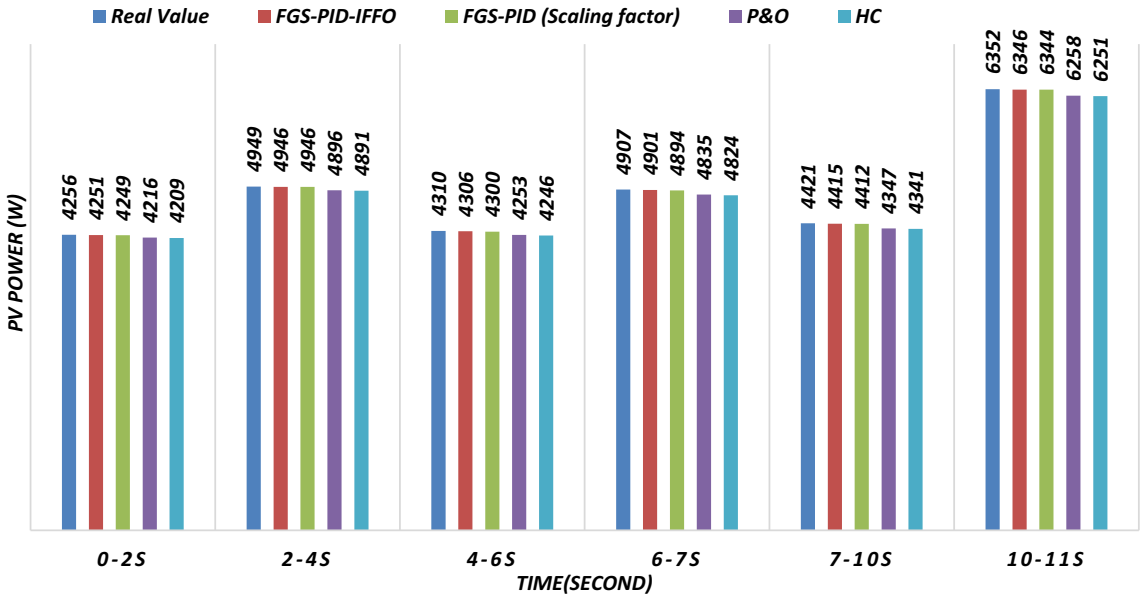

Fig. 11 PV power with different methods

$$H = \begin{cases} X_{\text{new}} = X_{ij} + \omega \times (X_{ij} - G_{\text{best}}(b)), & Q > \text{rand} \\ X_{\text{new}} = X_{ij} + r_3 \times (X_{ij} - G_{\text{best}}(b)), & \text{o.w.} \end{cases} \tag{17}$$

in which r_3 symbolizes a random value within the [0, 1] range, and w represents the fertility parameter of farmland decided at the start time, which is written as below:

$$\omega = \omega \times R_v, \quad 0 < R_v < 1 \tag{18}$$

Step 6) Final conditions: The potential solutions to the search space will be evaluated. In the course of this process, in the case of reaching the stopping criteria, the algorithm is terminated.

4.3 Improved IFFO technique

Even though, as a novel metaheuristic methodology, the FFO algorithm presents good results for the purpose of solving a variety of optimization-based applications [34, 35, and 36]; its major drawback is its inability to provide an appropriate convergence in such a way that it reaches premature convergence for a number of problems. Two modification mechanisms have been employed so as to solve this dilemma.

The first enhancement is the utilization of the Lévy flight (LF) mechanism, which has been used in a variety of metaheuristic techniques (Rajesh et al. 2015; Lu et al. 2021). A random walk approach is adopted in the Lévy flight in order to enhance the algorithm searchability, which is determined as below:

$$\text{LF}(w) \approx \frac{1}{\left(A \times |B|^{-\left(\frac{1}{\tau}\right)}\right)^{\tau+1}} \tag{19}$$

$$\sigma^2 = \left\{ \frac{\sin(\pi \times \tau/2)}{2^{(1+\tau)/2}} \times \frac{\Gamma(1+\tau)}{\tau \times \Gamma((1+\tau)/2)} \right\}^{2\tau^{-1}} \tag{20}$$

in which A,B $\sim$ N(0,σ^2) refers to the Lévy flight index (here,) (Li et al. 2018), and refers to the Gamma function.

By regarding the Lévy flight conception, the updated version of the equation for the composition of soil is presented below:

$$H = \begin{cases} X_{\text{new}} = X_{ij} + \omega \times (X_{ij} - G_{\text{best}}(b)) & , Q > \text{rand} \\ X_{\text{new}} = X_{ij} + Le(\delta) \times (X_{ij} - G_{\text{best}}(b)) & , \text{o.w.} \end{cases} \tag{21}$$

In addition, in the basic farmland fertility optimization, the parameter h varies within the [– 1, 1] range for the overall procedure of the optimization of the new solution.

The anti-cosine mechanism will be used here as the learning factor function as below:

$$h = h_{\min} + (h_{\max} - h_{\min}) \times \left(1 - \arccos\left(\frac{(-2 \times \frac{t}{T} + 1)}{\pi}\right)\right) \tag{22}$$

in which $h_{\max}$ and $h_{\min}$ stand for the maximum and the minimum h values, in which the initial value is [$h_{\min}$, $h_{\max}$] = [–1,1], T symbolizes the maximum quantity of iterations, and t symbolizes the number of the current iteration. Flowchart of farmland fertility is shown in Fig. 6.

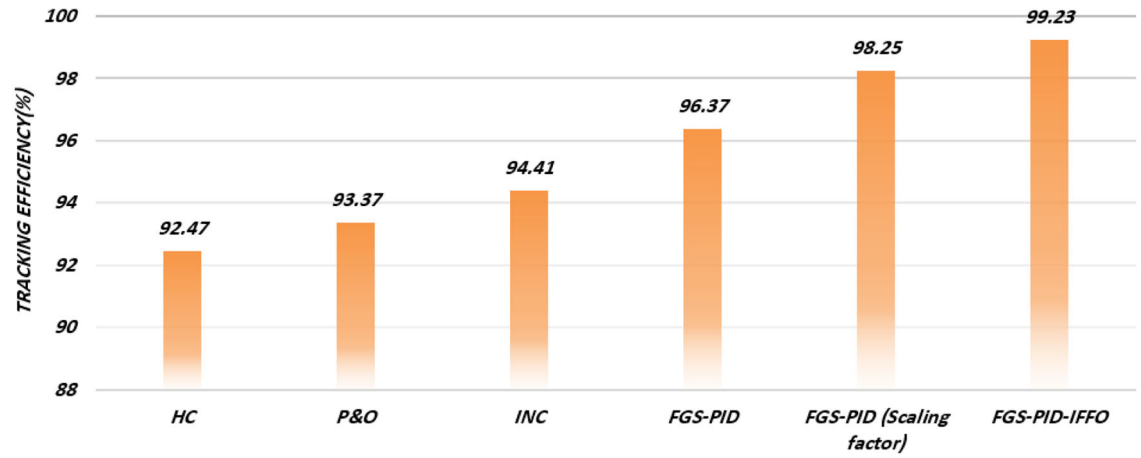

(a)

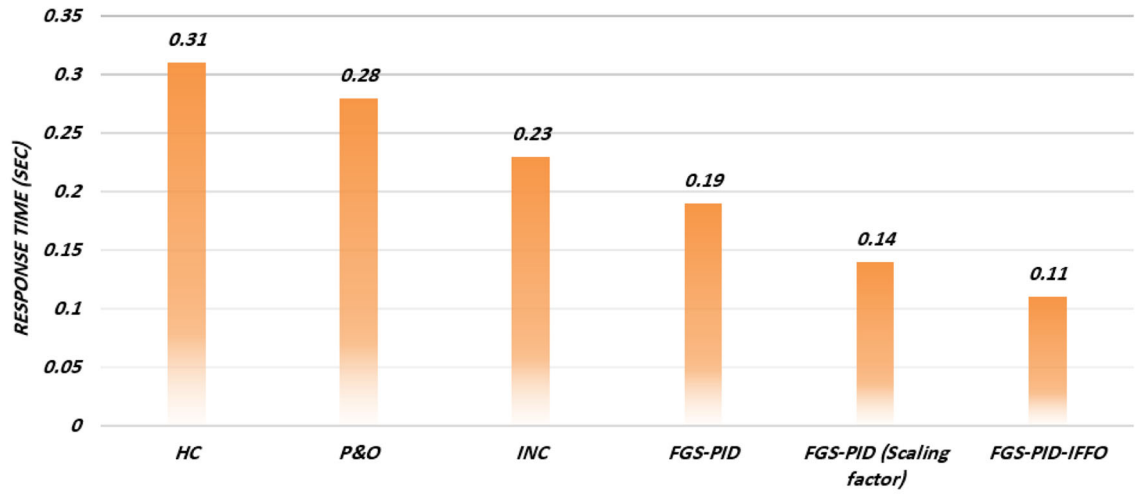

(b)

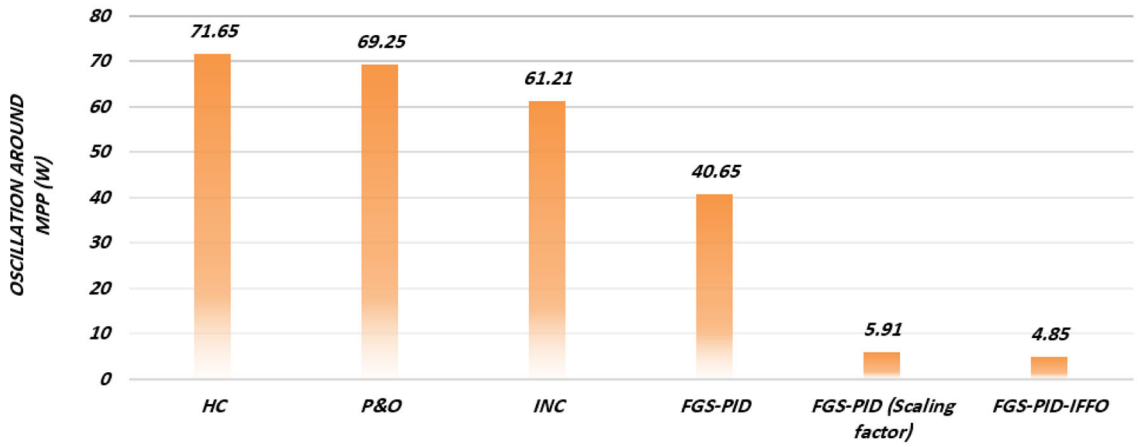

(c)

Fig. 12 **a** Efficiency; **b** Time response; **c** MPPT fluctuation

Table 3 Two scenarios of the PSCs

PSC number	Shading pattern
Scenario 1	[1000 880 550 390]
Scenario 2	[920 590 280 810]

Table 4 The designed MPPT approach

PSC number	Real value (W)	Achieved output power (W)
Scenario 1	184.1	182.3
Scenario 2	188.3	187.5

5 The WT model

This paper presents a uncomplicated mathematical model for the WT to establish the dynamic response of aerodynamic loading and multiple elements. Particularly, the complex simulators are substituted with a mathematical model with a straightforward structure to model a controller for WTs. A subset of nonlinear equations of ordinary differential (OD) type has been employed that has a limited degree of freedom which is used in this paper. The relation for the captured rotor aerodynamic power is as below [39]:

$$P_a = \frac{1}{2}\rho A R^2 C_p(\lambda, \beta')\upsilon^3 \tag{23}$$

where ρ indicates the density of air, the area of the blades is shown by A, υ is the wind speed (m/s), while P_a is aerodynamic power. Besides, the power coefficient shown by C_P highly relates to the pitch angle (β') and TSR (λ):

$$\lambda = \frac{\omega_r R}{\upsilon} \tag{24}$$

where the turbine speed is shown by ω_r and wind turbine blade radius is denoted by R. It should be noted here that the angle plays a key role in the WT controller. Figure 7a shows C_p-λ curves of the WT for different pitch angles (Mahmoud & Oyedeji, 2018). As can be seen, the tuning of pitch angle (β') would alter C_p. In contrast, controlling the pitch angle would adjust the WT's power output.

In this part, the suggested pitch angle control technique for the WT depicted in Fig. 7b and c is employed using PI and RBFNSM, respectively.

5.1 RBFNSM controller design

Figure 7d demonstrates the studied WT. The RBFNSM and PI controllers are represented with more detail in Hong and Chen (2014). The RBFN input acts as the switching function. It is worth noting that the sliding mode regulator is taken into account the output of the neural network. The RBFNSM framework would be implemented utilizing the self-learning option. Figure 7d illustrates the structure of this controller.

The sliding surface is stated as follows:

$$s(t) = ce(t) + \frac{\mathrm{d}}{\mathrm{d}t}e(t) \tag{25}$$

Pref is the reference wind power output, Pout shows the active power of the WT, while e denotes the error of tracking. The detailed formulations of the presented framework are as follows:

$$w_j(t) = w_j(t-1) + \eta.[y(t) - y_m(t)]h_j + \alpha[w_j(t-1) - w_j(t-2)] \tag{26}$$

$$\Delta b_j = [y(t) - y_m(t)]w_j h_j \frac{\|X - c_j\|^2}{b_j^3} \tag{27}$$

$$b_j(t) = b_j(t-1) + \eta\Delta b_j + \alpha.[b_j(t-1) - b_j(t-2)] \tag{28}$$

$$\Delta b_{ij} = [y(t) - y_m(t)]w_j \frac{x_j - c_{ij}}{b_j^2} \tag{29}$$

$$c_{ij}(t) = c_{ij}(t-1) + \eta\Delta c_{ij} + \alpha.[c_{ij}(t-1) - c_{ij}(t-2)] \tag{30}$$

In the above formulations, the momentum factor is denoted by α. Moreover, η describes the adaptive rate.

The next subsection describes the signal propagation and the basic function within every layer.

5.1.1 Layer 1

The node would be expressed as:

$$net_1^1 = s_1^1(k) \tag{31}$$

$$y_1^1(k) = f_1^1(net_1^1(k)) = net_1^1(k) \tag{32}$$

where $s_1^1(k)$ denotes the switching surface at iteration k.

5.1.2 Layer 2

The node would be expressed as:

$$net_j^2(k) = -\frac{\|s_1^2 - c_j\|^2}{b_j^2} \tag{33}$$

$$y_j^2 = f_j^2(net_j^2(k)) = \exp(net_j^2(k)), \quad j = 1, 2, ...m \tag{34}$$

In Eq. 34, the central vector and the base width constant relating to mode j are denoted by c_j and b_j, respectively, while b_j must be greater than zero.

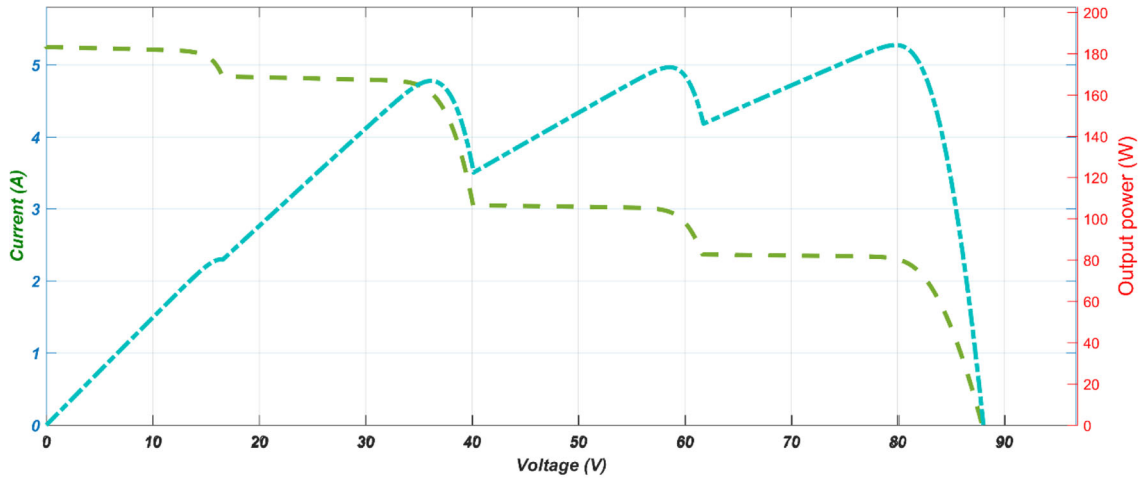

(a) SP1. PV power

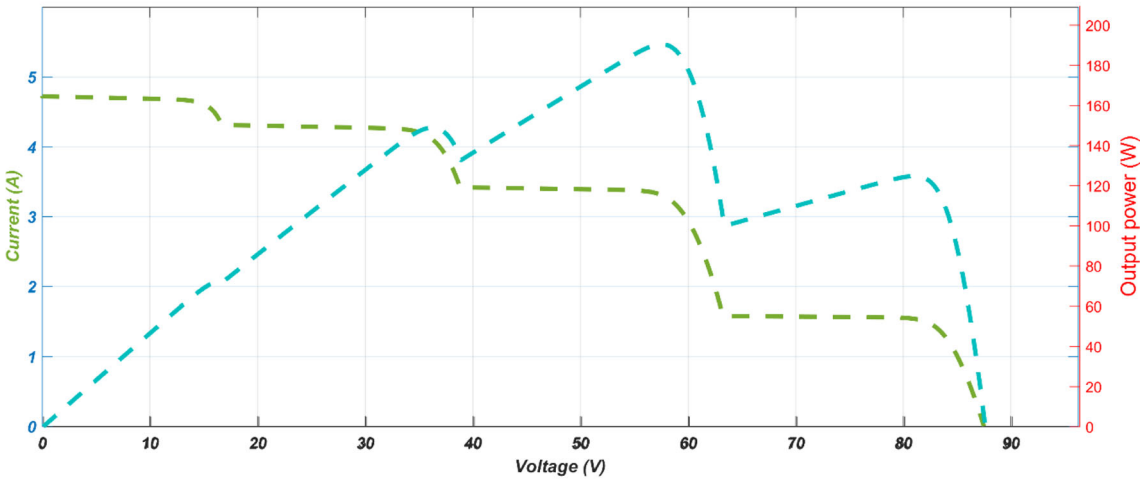

(b) SP2. PV power

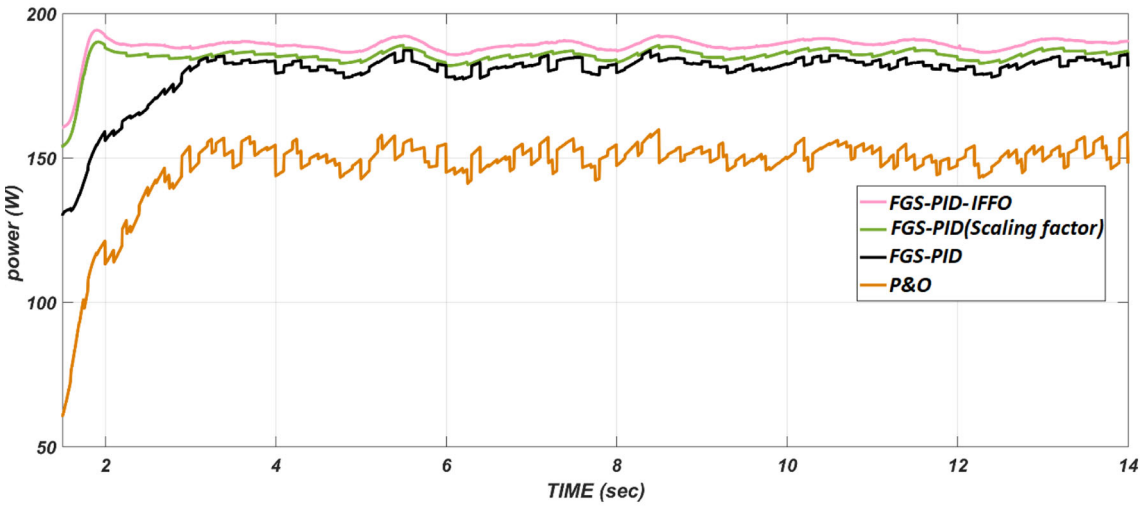

(c) SP2. Dynamic performance

Fig. 13 **a** SP1. PV power **b** SP2. PV power **c** SP2. Dynamic performance

Table 5 MPPT Comparison

Methods	FGS-PID(Scaling factor)	FGS-PID	PID	FLC	P&O	HC
Response time (S)	0.19	1.31	5.64	7.97	8.61	9.74
Oscillation (W)	3.25	7.91	10.47	14.65	16.87	18.97
Efficiency (%)	99.64	95.17	94.67	91.55	90.54	87.66

5.1.3 Layer 3

The node input and output are

$$net_0^3 = \sum_j w_j y_j^2(k) \tag{35}$$

$$y_0^3(k) = f_0^3(net_j^3(k)) = net_0^3(k) = \beta_c^{'} \tag{36}$$

where the RBFNSM's output is used as the pitch angle command of the suggested controller.

This study employs a supervised method for learning using the gradient descent to teach the system as the RBFNSM starts. The pattern used for adjusting the parameters w_j, c_{1j}, and b_{1j} of the RBFNSM is used.

6 System structure

The developed framework has been implemented in MATLAB/Simulink using an Intel Corei7 PC equipped with 8 GB RAM. Figure 8 illustrates the simulated system, including the PV and WT. The capacity of the studied PV is 7.3 kW comprising 81 modules with 9 by 9 arrangements, beside a 100 kW WT. It is also noted that the upstream grid is a 60 Hz 220 V system.

6.1 Effect of simultaneous irradiance and temperature

Figure 9a and b, in the present section, depicts the variations in temperature and irradiance. In accordance with Fig. 10a, the power tracker of the FGS-PID-IFFO technique showed high accuracy when addressing the valid direction as a result of its training and optimized tuning of the suggested model; however, that of the other MPPT technique was lost when the input irradiation underwent sudden variations. As Fig. 10b shows, given that the power output of the photovoltaic system is lower than its nominal capacity for solar irradiance, the grid should be capable of compensating for that. Figure 11 shows the generated power using the photovoltaic system by considering various solar irradiance values.

The MPPT efficiency equation is employed as shown in Eq. 37:

$$\eta.MPPT_{(\text{Average})} = \frac{\int P_{\text{out}}(t)\mathrm{d}t}{P_{\max}(t)\mathrm{d}t} \tag{37}$$

in which $P_{\max}$ and P_{out} stand for the theoretical and actual power of the photovoltaic array, respectively. By employing the simulated current and voltage of the photovoltaic array, the actual photovoltaic power was decided, which was then multiplied. Even though under various climatic conditions, the efficiency of the FGS-PID-IFFO technique reached an average efficiency of 99.3%, as shown in Fig. 12a, it was within the 92.5–99.87% range for the other techniques. As illustrated in the zoomed section of Fig. 12b, the time required for reaching convergence for the power tracker in the FGS-PID-IFFO technique is the maximum in comparison with the other techniques, being 0.07, 0.11, and 0.13 s, approximately. In addition, given that it showed the minimum smooth fluctuation around the MPP for the steady state, it results in shortened computation time, as depicted in the zoomed-in part of Fig. 12c.

6.2 Partial shading conditions

In the characteristic curve, more than one peak point occurs in the case of uneven solar irradiance received by the photovoltaic modules, which imposes difficult operating circumstances for the maximum power point tracking algorithm. Table 3 represents two scenarios adopted in order to study the contribution of the partial shading conditions (PSCs) to the system's performance. One can generally group the mentioned peak points as global and local maxima. The system's operation subject to the designed maximum power point tracking control strategy under partial shading conditions has been evaluated, the results of which are shown in Table 4. According to the first scenario, the solar irradiance values are 1.0, 0.88, 0.55, and 0.39 KW/m^2. The P–V and I–V plots are shown in Fig. 13a and include three local maxima in addition to a global maximum, the value of which is 182.3 W, obtained on point 4. From another perspective, in the second scenario, the assumed values of the solar irradiance are 0.92, 0.59, 0.280, and 0.81 kW/m^2, and Fig. 13b illustrates the associated results. In this regard, the global maximum attained on point 3 is equal to 187.5 W. According to the acquired results, the suggested FGS-PID-IFFO technique provides excellent performance for the system in reaching the global maximum; however, other techniques resulted in a local maximum at 145.5 W. This implies that the application of these techniques may result in higher power losses. The dynamic response of the investigated

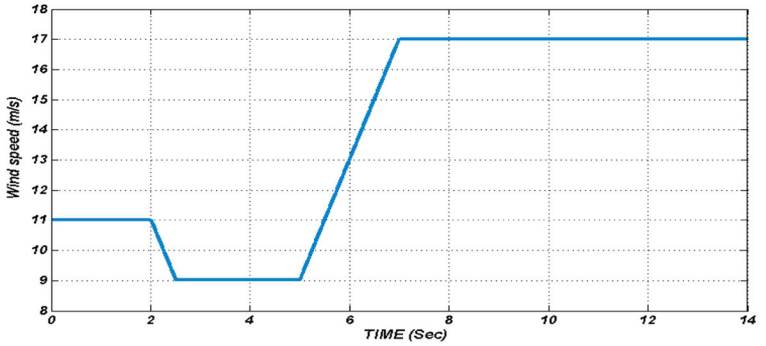

(a)

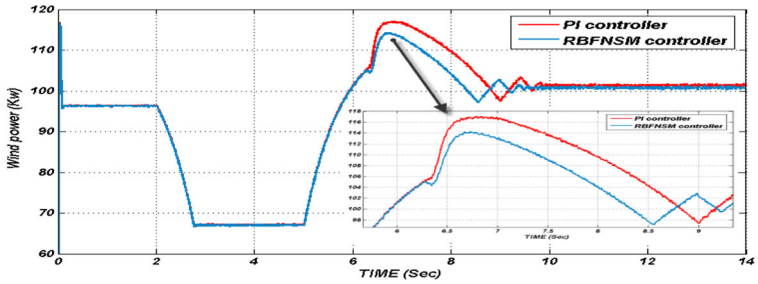

(b)

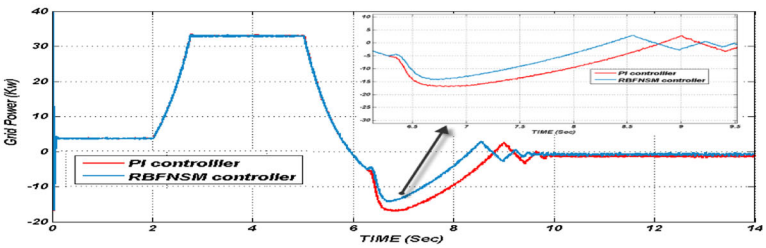

(c)

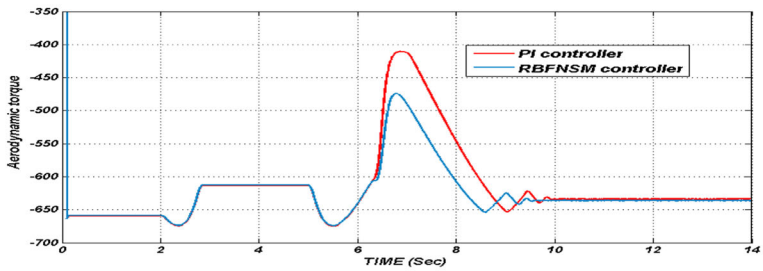

(d)

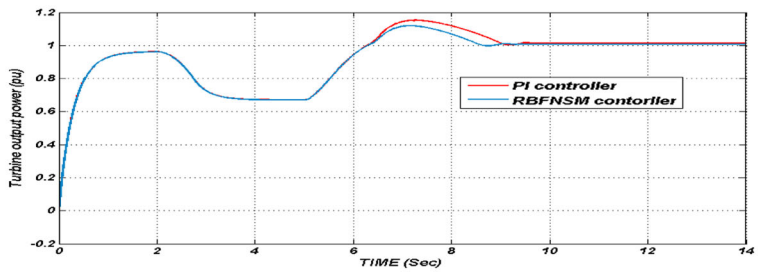

(e)

Fig. 14 Simulated results for the WT: **a** Wind speed; **b** Wind power; **c** Grid power; **d** Aerodynamic torque; **e** Turbine output power

techniques is illustrated in Fig. 13c. It is evident that the suggested FGS-PID-IFFO technique presents a superb performance at minimum fluctuations. In addition, Table 5 is devoted to the comparison made between the above-mentioned control strategies by means of addressing the response time, oscillations, and the efficiency of tracking, which shows that this framework could supply 99% efficiency compared to the efficiency of 95–97% presented by other techniques.

6.3 Wind speed variations

WT's pitch angle responses are determined in phase of fixed load and variable wind speed, while the rated speed is 12 m/s. The speed of wind over $0 < t < 2$ is 11 m/s, and at $t = 2$ (sec), it reduces to 9 m/s. After that, at $t = 5$, it dramatically increases to 17 m/s, as shown in Fig. 14a.

Simulation results of wind power in Fig. 14b show that in case of using the RBFNSM controller above the rated speed, the WT's output increases by substantially raising the wind speed; then, it reduces to the rated power and becomes smoother that leads to preventing any mechanical fatigue to the generator in comparison with the PI controller.

As shown in Fig. 14b, c, d, and e, the pitch angle control's aim is to optimize the WT's output. For the speeds lower than the nominal speed, the pitch should be optimally adjusted to result in the highest power level and avoiding the input electrical power to surpass the limitations. For the speeds greater than the nominal speed, controlling the pitch angle would lead to efficiently controlling the aerodynamic power caused by the rotor, while it minimizes mechanical fatigue to the generator. Contrarily, in the high wind speed situation, although the available wind power is higher than the rated value, the pitch angle is regulated to keep the generated power at just rated one, not to maximize it. This is done to protect the wind turbine structurally and avoid catastrophic operation. So, the obtained results verify the better performance of the RBFNSM controller compared to prevalent pitch angle control techniques in terms of lower mechanical fatigue to the generator, lower power peak, and lower torque peak. The speed of wind during $0 < t < 5$ is less than 12 m/s; accordingly, WT's power is below 100 kW, and the grid supplies the required power as shown in Fig. 14c.

7 Conclusion

The output power obtained from each solar cell is directly affected by the intensity of the solar radiation, while it is conversely related to the temperature and irradiance, and both of these parameters are subjected to changes over time. As a result, MPP tracking techniques must be used to overcome such changes. In order to regulate the MFs of FGS, the FLC and developed IFFO algorithm are used. Moreover, the pitch angle control is applied for the WT. The pitch angle control of the WT is implemented by the RBFNSM to control the generated power and the speed at the nominal value. This algorithm has a great ability to regulate the triangular MFs of the inputs and output, automatically as well as the pitch angle is regulated to restrict the generated power and the speed at the nominal value. This is done to protect the wind turbine structurally and avoid catastrophic operation. The results derived and reported in the paper verified the performance of the developed frameworks. Furthermore, the proposed strategy also shows good dynamic response beside boosted stability results in transferring power between the upstream system and the hybrid generating system.

Acknowledgements This work was supported by Foundation of State Key Laboratory of Public Big Data (No.2023004), National Natural Science Foundation of China (No.61862051), the Science and Technology Foundation of Guizhou Province (No. ZK[2022]549), the Natural Science Foundation of Education of Guizhou province (No. [2019]203, No. KY[2019]067), and the Funds of Qiannan Normal University for Nationalities (No.qnsy2019rc09).

Funding This study was not funded any institution and organization.

Data availability Enquiries about data availability should be directed to the authors.

Declarations

Conflict of interest Author declares that he has no conflict of interest.

Research involving human participants and/or animals This article does not contain any studies with human participants performed by any of the authors.

Informed consent The process of program coding, numerical execution, and statistical analysis was based on personal computers. All authors agreed to publish this paper, if accepted.

References

Agwa AM, El-Fergany AA, Maksoud HA (2020Aug) Electrical characterization of photovoltaic modules using farmland fertility optimizer. Energy Convers Manage 1(217):112990

Ahmadi S, Abdi S, Kakavand M (2017) Maximum power point tracking of a proton exchange membrane fuel cell system using PSO-PID controller. Int J Hydrogen Energy 42(32):20430–20443

Benadli R, Sellami A. Sliding mode control of a photovoltaic-wind hybrid system. In2014 International Conference on Electrical Sciences and Technologies in Maghreb (CISTEM) 2014 Nov 3 (pp. 1–8). IEEE.

Chopra S, Mitra R, Kumar V. Identification of Self-Tuning Fuzzy PI type controllers with reduced rule set. InProceedings. 2005 IEEE

Networking, Sensing and Control, 2005. 2005 Mar 19 (pp. 537–542). IEEE.
Chopra S, Mitra R, Kumar V. Auto tuning of fuzzy PI type controller using fuzzy logic. International journal of computational cognition (http://www.ijcc.us). 2008 Mar;6(1).
Dadfar S, Wakil K, Khaksar M, Rezvani A, Miveh MR, Gandomkar M (2019) Enhanced control strategies for a hybrid battery/photovoltaic system using FGS-PID in grid-connected mode. Int J Hydrogen Energy 44(29):14642–14660
Elgendy MA, Zahawi B, Atkinson DJ (2012) Assessment of the incremental conductance maximum power point tracking algorithm. IEEE Trans Sustain Energy. 4(1):108–17. https://doi.org/10.1109/TSTE.2012.2202698
Hai T, Wang D, Muranaka T (2022) An improved MPPT control-based ANFIS method to maximize power tracking of PEM fuel cell system. Sustain Energ Technol Assessments 1(54):102629
Harrag A, Messalti S (2015) Variable step size modified P&O MPPT algorithm using GA-based hybrid offline/online PID controller. Renew Sustain Energy Rev 1(49):1247–1260
Hong CM, Chen CH (2014) Intelligent control of a grid-connected wind-photovoltaic hybrid power systems. Int J Electr Power Energy Syst 1(55):554–561
Hosseini SM, Rezvani A (2020) Modeling and simulation to optimize direct power control of DFIG in variable-speed pumped-storage power plant using teaching–learning-based optimization technique. Soft Comput 24:16895
Izadbakhsh M, Rezvani A, Gandomkar M (2015) Dynamic response improvement of hybrid system by implementing ANN-GA for fast variation of photovoltaic irradiation and FLC for wind turbine. Arch Electr Eng 64(2):291–314
Khan MJ, Mathew L (2021) Artificial neural network-based maximum power point tracking controller for real-time hybrid renewable energy system. Soft Comput 25(8):6557–6575
Kumar M, Sandhu KS, Kumar A. Simulation analysis and THD measurements of integrated PV and wind as hybrid system connected to grid. In2014 IEEE 6th India International Conference on Power Electronics (IICPE) 2014 Dec 8 (pp. 1–6). IEEE.
Leng H, Li X, Zhu J, Tang H, Zhang Z, Ghadimi N (2018) A new wind power prediction method based on ridgelet transforms, hybrid feature selection and closed-loop forecasting. Adv Eng Inform 1(36):20–30
Li X, Niu P, Liu J (2018) Combustion optimization of a boiler based on the chaos and Levy flight vortex search algorithm. Appl Math Model 1(58):3–18
Li X, Wen H, Hu Y, Jiang L (2019) A novel beta parameter based fuzzy-logic controller for photovoltaic MPPT application. Renew Energy 1(130):416–427. https://doi.org/10.1016/j.renene.2018.06.071
Lu X, Li B, Guo L, Wang P, Yousefi N (2021) Exergy analysis of a polymer fuel cell and identification of its optimum operating conditions using improved Farmland Fertility Optimization. Energy 216:119264
Luo L, Abdulkareem SS, Rezvani A, Miveh MR, Samad S, Aljojo N, Pazhoohesh M (2020) Optimal scheduling of a renewable based microgrid considering photovoltaic system and battery energy storage under uncertainty. J Energy Storage 1(28):101306
Mahmoud MS, Oyedeji MO (2018) Continuous-time multi-model predictive control of variable-speed variable-pitch wind turbines. Int J Syst Sci 49(11):2442–2453
Mudi RK, Pal NR (1999) A robust self-tuning scheme for PI-and PD-type fuzzy controllers. IEEE Trans Fuzzy Syst 7(1):2–16
Ogata K, Yang Y (2002) Modern control engineering. Prentice hall
Oskouei AB, Banaei MR, Sabahi M (2016) Hybrid PV/wind system with quinary asymmetric inverter without increasing DC-link number. Ain Shams Eng J 7(2):579–592
Parida A, Chatterjee D (2016) Cogeneration topology for wind energy conversion system using doubly-fed induction generator. IET Power Electronics 9(7):1406–1415
Radhika A, Soundradevi G, Kumar RM (2020) An effective compensation of power quality issues using MPPT-based cuckoo search optimization approach. Soft Comput 24(22):16719–16725
Hai T, Alazzawi AK, Zhou J, Farajian H (2023) Performance improvement of PEM fuel cell power system using fuzzy logic controller-based MPPT technique to extract the maximum power under various conditions. Int J Hydrogen Energy 48(11):4430–45
Rajesh K, Kulkarni AD, Ananthapadmanabha T (2015) Modeling and simulation of solar PV and DFIG based wind hybrid system. Procedia Technol 1(21):667–675
Sabo A, Wahab NI, Othman ML, Jaffar MZ, Beiranvand H (2020) Farmland fertility optimization for designing of interconnected multi-machine power system stabilizer. Appl Modell Simul 12(4):183–201
Sabo A, Wahab NI, Othman ML, Zurwatul M, Jaffar AM (2020) Novel farmland fertility algorithm based PIDPSS design for SMIB angular stability enhancement. Int J Adv Sci Technol 29(6):873–882
Salameh ZM, Dagher F, Lynch WA (1991) Step-down maximum power point tracker for photovoltaic systems. Sol Energy 46(5):279–282
Sera D, Mathe L, Kerekes T, Spataru SV, Teodorescu R (2013) On the perturb-and-observe and incremental conductance MPPT methods for PV systems. IEEE J Photovoltaics 3(3):1070–1078
Shayanfar H, Gharehchopogh FS (2018) Farmland fertility: a new metaheuristic algorithm for solving continuous optimization problems. Appl Soft Comput 1(71):728–746
Shengqing L, Fujun L, Jian Z, Wen C, Donghui Z (2020) An improved MPPT control strategy based on incremental conductance method. Soft Comput 24(8):6039–6046
Veeramanikandan P, Selvaperumal S (2021) Investigation of different MPPT techniques based on fuzzy logic controller for multilevel DC link inverter to solve the partial shading. Soft Comput 25(4):3143–3154
Yin N, Abbassi R, Jerbi H, Rezvani A, Müller M (2021) A day-ahead joint energy management and battery sizing framework based on θ-modified krill herd algorithm for a renewable energy-integrated microgrid. J Clean Prod 1(282):124435
Zhao ZY, Tomizuka M, Isaka S (1993) Fuzzy gain scheduling of PID controllers. IEEE Trans Syst, Man, Cybernet 23(5):1392–1398